Inertia Friction Welding Dissimilar Nickel-Based Superalloys Alloy 720Li to IN718

Z.W. HUANG, H.Y. LI, M. PREUSS, M. KARADGE, P. BOWEN, S. BRAY, and G. BAXTER

This article describes a comprehensive microstructural characterization of an inertia friction welded joint between nickel-based superalloys 720Li and IN718. The investigation has been carried out on both as-welded and postweld heat-treated conditions. The detailed metallographic analysis has enabled the relation of hardness profiles across inertia-welded alloy 720Li to IN718 and morphological changes of the precipitates present. The work demonstrates that inertia friction welding (IFW) 720Li to IN718 results in a weld free of micropores and microcracks and no significant chemical migration across the weld line. However, substantial differences in terms of grain structure and precipitation phase distribution variations are observed on each side of the dissimilar weld. The high γ' volume fraction alloy 720Li exhibits a wider heat-affected zone than the mainly γ'' strengthened IN718. Alloy 720Li displays only a small hardness trough near the weld line in the as-welded condition due to the depletion of γ', while γ''-strengthened IN718 shows a soft precipitation-free weld region. Postweld heat treatment (PWHT) of the dissimilar weld at 760 °C, a typical annealing temperature for alloy 720Li, results in an overmatch of the heat-affected zone in both sides of the weld. The comparison of the as-welded and postweld heat-treated condition also reveals that IN718 is in an overaged condition after the stress relief treatment.

DOI: 10.1007/s11661-007-9194-6

I. INTRODUCTION

INERTIA friction welding (IFW) is a solid-state welding process, which allows joining nickel-base superalloys with a high γ' volume fraction or different types of nickel-base superalloys. During IFW, one part is attached to a rotating flywheel, while the second, nonrotating part is forced into contact with the rotating one under hydraulic pressure. The kinetic energy stored in the rotating flywheel is then transformed into heat at the interface of the two parts. In this way, a sufficiently high temperature is produced at the interface, which, together with the torsional forces and axial pressure, results in material being ejected, and a bond is formed. The IFW is considered an attractive manufacturing process because of its suitability for mass production. More importantly, unlike electron beam welding, laser welding, and other welding technologies, the IFW process is a solid-state joining process. As a result, problems related to liquation such as occurrence of microfissures,[1,2,3] precipitation of detrimental phases, intergranular hot cracking,[4–7] and porosity[8] can be either avoided or diminished. As a consequence, high γ' volume fraction nickel-base superalloys, considered to be unweldable by fusion welding techniques, can be joined by IFW. The IFW is widely used in the automotive and power generation industry.[9,10] In the aeroengine industry, it is mainly used to join high-temperature materials such as titanium and nickel-base superalloys.[11,12]

The IFW of two different types of nickel-base superalloys, namely, alloy 720Li to IN718, has been undertaken in this study. Such dissimilar joints are highly attractive for the aeroengine industry as they result in significant weight reductions while maintaining the mechanical properties and required temperature capability. The aim of this study is to improve the understanding of inertia friction joining two types of high-temperature alloys by mapping microhardness and microstructure variations across the weld region of the dissimilar material combination.

Previous microstructural characterization of similar friction-welded nickel-base superalloys has demonstrated that, due to the thermal history and heavy plastic deformation in the near weld region, a dramatic variation of the microstructure is observed, resulting in partial or full dissolution of γ' precipitates in this region.[12,13] Dissolution of γ'' in this region is also expected, because the temperature reached near the weld line is in the range of the forging temperature.[9] Studies focusing on the residual stress characterization of such inertia friction welds have highlighted the high levels of tensile stresses observed in the weld region and the importance of developing an appropriate stress relief temperature.[14,15] The present work is one of the first

Z.W. HUANG, Senior Research Fellow, H.Y. LI, Research Fellow, and P. BOWEN, Professor, are with the Department of Metallurgy and Materials, School of Engineering, The University of Birmingham, Birmingham B15 2TT, United Kingdom. Contact e-mail: z.w.huang@bham.ac.uk M. PREUSS, Lecturer in Materials Performance, and M. KARADGE, Research Fellow, are with the School of Materials, University of Manchester, Manchester, M1 7HS, United Kingdom. S. BRAY, Friction Welding Sprcialist and G. BAXTER, Intertia Welding Sprcialist, are with Rolls-Royce plc., Elton Road, Derby DE24 8BJ, United Kingdom.

Manuscript submitted June 15, 2006.
Article published online June 26, 2007.

Table I. Chemical Compositions of the Nickel-Based Superalloys Used for IFW in This Work (Weight Percent, Balance Nickel)

Alloy	Fe	Cr	Mo	Nb	Co	Ti	Al	W	Si	C	B
U 720Li	—	16	3	—	15	5.0	2.5	1.25	—	0.015	0.015
IN718	17.95	17.82	2.92	5.39	0.13	0.99	0.50	—	0.07	0.024	0.004

metallurgical studies of a dissimilar nickel-base inertia friction weld. The metallurgical evaluation of inertia friction-welded alloy 720Li to IN718 has been carried out on both as-welded and postweld heat-treated (PWHT'd) conditions. The weld assessment includes microhardness mapping and metallographic analysis of the heat-affected zone and the parent material. The microstructural characterization of the γ grain structure was carried out using electron backscatter diffraction (EBSD). Field emission gun scanning electron microscopy (FEGSEM), transmission electron microscopy (TEM), and energy-dispersive X-ray (EDX) microanalysis were undertaken to characterize the coherent strengthening phases γ' and γ''. The extensive microstructural mapping employed in this investigation has provided a detailed explanation of the metallurgy across the weld line and near weld line regions in alloy 720Li to IN718, relating the hardness profiles to the distribution and morphology of the precipitates present.

II. EXPERIMENTAL

A. *Materials and Specimens*

Alloy 720Li is an advanced nickel-based superalloy. Its superior mechanical properties are achieved through the precipitation of about 45 vol pct γ' (Ni_3(Ti,Al) with a $L1_2$ structure) from supersaturated γ matrix. The γ' in 720Li consists of primary, secondary, and tertiary γ', defined based on its size. The primary γ' remains undissolved during solution treatment. It lies at the γ grain boundaries and can prevent γ grain growth. Secondary and tertiary γ' form on cooling and normally have a size greater than 100 nm and less than 50 nm, respectively. The bimodal distribution of intragranular γ' is the main source of strengthening. IN 718 is a versatile nickel-based superalloy strengthened by a combination of γ'' (Ni3(Nb), a DO_{22} structure, and γ' precipitates. Both are nanometer-sized precipitates. The volume fraction ratio of γ'' to γ' is determined mainly by relative contents of Al + Ti over Nb and normally can attain the ratio of 3 to 4. In addition, a more stable δ phase (Ni_3(Nb) with an orthorhombic DO_a structure) can be observed in the γ matrix of IN 718. This phase has a size of a few microns and mainly decorates γ grain boundaries, capable of controlling grain growth during forging.

Alloy 720Li and IN718 rings used for IFW were machined from large-scale forgings. The chemical composition of the two alloys is given in Table I. A sub-γ' solvus heat treatment at 1105 °C for 4 hours was carried out on alloy 720Li, while a sub-δ solvus heat treatment at 980 °C for 1 hour was carried out on IN718. In order to reduce the residual stresses of the forgings prior to machining, both forgings were stress-relief annealed. For this study, rings of the two alloys, with an outer diameter of 143 mm and a wall thickness of 25 mm for U 720Li and 20 mm for IN 718, were machined and then inertia friction welded at MTI (South Bend, IN). Slices for microstructural studies were machined from the welded ring along the axial direction, using electrodischarge machining (EDM). Postweld heat treatments (PWHTs) were conducted on these slices in an air-circulating furnace at 760 °C for 2, 4, 8, and 24 hours, followed by air cooling to room temperature.

B. *Microhardness Testing*

Vickers microhardness testing was carried out under a load of 1 kg using a calibrated Vickers-hardness indentation machine. Microhardness testing was undertaken on the plane defined by the axial and radial directions. For each sample, the specific testing was done in the middle region of the weld and on a grid of five lines parallel to the axial direction, spaced greater than five indentations apart. Measurements were taken from the weld line (with some additional measurement point across the weld line to ensure the exact position of it) to a distance of 10 mm away from it. The axial distance of the indentation marks was controlled with a micrometer. The results presented are the average of the five measurements per axial position. The average standard deviation of the microhardness values was 7.2 (HV1) in alloy 720Li and 6.6 (HV1) in IN718.

C. *SEM and Image Analysis*

High-resolution FEGSEM studies on samples etched according to Preuss *et al.*[12] enable the study of γ' with a size of only a few nanometers. Characterization of the γ' distribution for various distances from the weld line was undertaken using a FEGSEM (PHILIPS* XL 30) operating at 8 kV and secondary electron mode. The hardness indentation marks were used as distance reference points for each axial position. The composition of the γ' etchant is given in Table II. This etchant dissolves γ' precipitates from the polished surface and leaves the γ-matrix intact. In this way, it is possible to characterize size distribution and volume fraction of γ' by simply characterizing the holes left behind from the dissolved γ' precipitates. Because nickel-base superalloys generally exhibit bi-modal or tri-modal γ' distributions,[16,17] it is necessary to study the material at different magnifications. At each axial position and for each magnification, five images were taken, which were subsequently analyzed.

*PHILIPS is a trademark of Philips Electronic Instruments Corp., Mahwah, NJ.

Table II. Chemical Composition of the γ' Etchant

Part I	Part II
150 mL H_2O	15 mL HNO_3
150 mL HCL	25 mL H_2O
2.5 g MoO_3	30 mL Part I

The particle size and volume fraction of the coarse, intergranular γ', often referred to as primary γ', was carried out using a mean linear-intercept method. The intragranular secondary and tertiary γ' were analyzed using the image analysis software package Kontron KS 400 (Image Associates Ltd, Bicester, UK). For the quantitative analysis of ultra-fine γ' precipitates, which were found in the heat-affected zone (HAZ) of alloy 720Li, a high-resolution FEGSEM (FEI Sirion) based at the University of Manchester was facilitated. This microscope is equipped with a through lens detector, which operates at 5 kV and provides a maximum resolution of 2 nm. Images taken on the FEI Sirion were also quantitatively analyzed using the image analysis package Kontron KS 400. The average accuracy of the γ' volume fraction was determined by calculating the average value of the standard deviations for every γ' family. This has been previously shown.

D. *EDX Microanalysis*

The EDX spot microanalysis was carried out in the γ matrix grains at the weld line to determine the compositional change across the weld line, using a PHILIPS XL 30 scanning electron microscope fitted with a LINK ISIS analytical EDX microanalyzer (Oxford Instruments NanoAnalysis, High Wycombe, UK). The EDX system was calibrated to a standard nickel sample before collecting data. The spot analysis of the chemical composition was conducted using an accelerating voltage of 20 kV and a spot size 5. The smallest step size used was 2 μm in the near weld line region. It is well documented that the spatial range of electron interaction volume, which decides the accuracy of compositional analysis, depends mainly on the accelerating voltage and the elements in the specimen to be analyzed. With an accelerating voltage of 20 kV and zero tilt, calculation of the spatial range on either side of the bond line gives a resolution of 1.29 μm for IN718 and 1.35 μm for alloy 720Li.

E. *Transmission Electron Microscopy*

The TEM investigations of microstructural features, such as γ', γ'', and dislocation structures, were carried out using a PHILIPS CM 20 transmission electron microscope operating at 200 kV. A slice of 4 mm in thickness was cut from the axial direction of the welded ring using EDM, which was subsequently turned into a 3-mm diameter bar using a lathe. A brief electropolishing and etching procedure of the 3-mm-diameter bar was used to reveal the weld line and enable accurate positioning of the cutting wheel in respect to the weld line. Disks of ~200 μm in thickness were cut from the bar using a diamond coated wheel and then subjected to twin-jet electrochemical polishing using an electrolyte of 12 pct perchloric acid in methanol for IN718 and an electrolyte of 20 pct perchloric acid in methanol for alloy 720Li. The axial position of a TEM specimen relative to the weld line was determined by measuring the distance between the weld line and the cutting position and adding one half of the disk thickness (normally ~100 μm), assuming that the thin area under TEM examination is located in the middle of the disk produced. Quantitative analysis of the volume fraction of γ'' in IN718 was carried out on TEM centered dark-field (CDF) images, based on the measured foil thickness, which was calculated using the thickness fringes and extinction distance **g** (for Ni with **g** vector of 200, using $\mathbf{g} = 27.5$ nm). The invisibility of γ'' under a specific **g** vector was also taken into account when doing the image analysis of TEM CDF photographs for the volume fraction of γ''. Similar to the quantitative analysis on γ' particles, the average accuracy of the γ'' volume fraction and the size is determined by calculating the average value of the standard deviations.

F. *Electron Backscatter Diffraction*

The EBSD mapping at different positions across the weld was carried out on a PHILIP XL 30 FEGSEM equipped with a state-of-the-art EBSD system and Flamenco software at the Manchester Materials Science Centre (Manchester, United Kingdom). The EBSD patterns were detected by using a charge-coupled device camera and image-processed background subtraction. Because no grain size variation or recrystallization is expected to take place during postweld heat treating the joint material at 760 °C, only the as-welded condition was mapped. Ten area maps were acquired from the weld line to the parent material of each alloy using a scanning step size between 0.15 and 0.75 μm for each map. The EBSD data were analyzed using VMAP, an analysis software developed by Humphreys *et al.*,[18] to obtain the grain size, orientation distribution, and stored energy. The microstructure was reconstructed from the orientation data, and the mean grain diameter ($\overline{D}$) was determined for each map from the "mean linear intercept distance" (MLI) according to $\overline{D} = 1.5$ MLI. Each orientation map contained at least 1200 grains. The stored energy was determined for each map to assess the level of plastic deformation experienced by the material at different axial positions. The stored energy was calculated for each map by determining the degree of misorientation within each grain. The method assumes that all the energy stored in the material is in the form of low- or high-angle boundaries of energy γ and that the contribution from free dislocations is negligible. The method also assumes that the boundaries are stable low-energy boundaries whose energies γ can be calculated from the Read–Shockley equation if the boundary misorientation θ is known:

$$\gamma = \gamma_m \frac{\theta}{\theta_m}\left(1 - \ln\frac{\theta}{\theta_m}\right) \qquad [1]$$

where γ_m is the energy of a high-angle boundary and θ_m is the misorientation at which a boundary is considered to be a high-angle boundary (typically 15 deg).

III. RESULTS AND DISCUSSION

A. *Metallurgical Features across the Weld Line*

Examples of the γ grain distribution and the coarse precipitates in alloy 720Li and IN718 are shown for the near the weld line region (as-welded condition) in Figures 1(a) and (c) and for parent alloys in Figures 1(b) and (d), respectively. These SEM images show that alloy 720Li forms a primary γ'-free zone between the weld line and 300 μm from it (Figure 1(a)), whereas IN718 displays a δ-free zone half the size (Figure 1(c)). Figure 1(d) also shows coarse carbides in the parent IN718. Near the weld line, more retained primary carbides were found in IN718 than in alloy 720Li (Figures 1(a) and (c)), which seems to be related to the higher levels of carbon in IN718 than in alloy 720Li (Table I). Table I and Figures 1(a) and (c) also display equiaxed grains in the near weld line region, indicating that the microstructure has recrystallized during the welding process. (A more detailed analysis using EBSD can be found in Section F). Under equilibrium conditions, the γ'-solvus in alloy 720Li has been reported to be around 1150 °C.[16,19] Under fast heating conditions, such as 300 °C s^{-1}, superheating effects have been observed in Astroloy (nickel-base superalloys similar to alloy 720Li), which increases the γ'-solvus by about 125 °C[16] due to a kinetic effect. However, recent results of process modeling of IFW of RR1000 (powder metallurgical nickel-base superalloy, about 48 vol pct γ') suggest that heating rates are significantly less severe than 300 °C s^{-1} in the IFW process, and therefore, the actual maximum temperature in alloy 720Li near the weld line might be relatively close to the equilibrium γ'-solvus.[20] Brooks reported a δ-solvus temperature of 1000 °C for IN718 under equilibrium conditions.[21] At such a temperature, the main strengthening precipitates γ'' in IN718 as well as γ' were expected to be completely dissolved. Once the strengthening precipitates have been dissolved it is reasonable to assume that the material will exhibit a very low flow stress and material will be ejected into the flash. As a result, microstructures and macrostructures characteristic of different maximum temperatures in the near weld line region can be expected on either side of the weld: IN718 will be ejected from the weld region into the flash at a lower temperature than alloy 720Li, which is expected to be exposed to a higher temperature and longer time than IN718. Macroscopic studies of the weld region revealed that a thicker flash was ejected from the IN 718 side than from the alloy 720Li side. The average thickness of the flash was measured to be 5.0 mm for IN 718 and 1.5 mm for alloy 720Li under the present condition. This can be explained by the different high-temperature mechanical properties of the two alloys with IN718 dropping strength more quickly than alloy 720 Li in the high-temperature region.

B. *Compositional Change across the Weld Line*

The EDX microanalysis was conducted in γ grains at the weld line to determine the compositional change across the weld line. As shown in Figure 2(a), a relatively large grain (labeled as grain G) extends across the weld line. Spot analyses of the composition were carried out on both sides at 2 to 50 μm from the weld line. As indicated in Figure 2(a), the first three spots were analyzed inside the grain G with a step size of 2 μm. The fourth analysis was conducted at 10 μm and the fifth at 15 μm from the weld line, respectively, in neighboring grains. Spot analyses 6/–6 were done at 50 μm from the weld line, which is located outside Figure 2. Several scans across the weld line were conducted in this manner. Typical element profiles (Fe, Co, Nb, and Ti) across the weld line were plotted

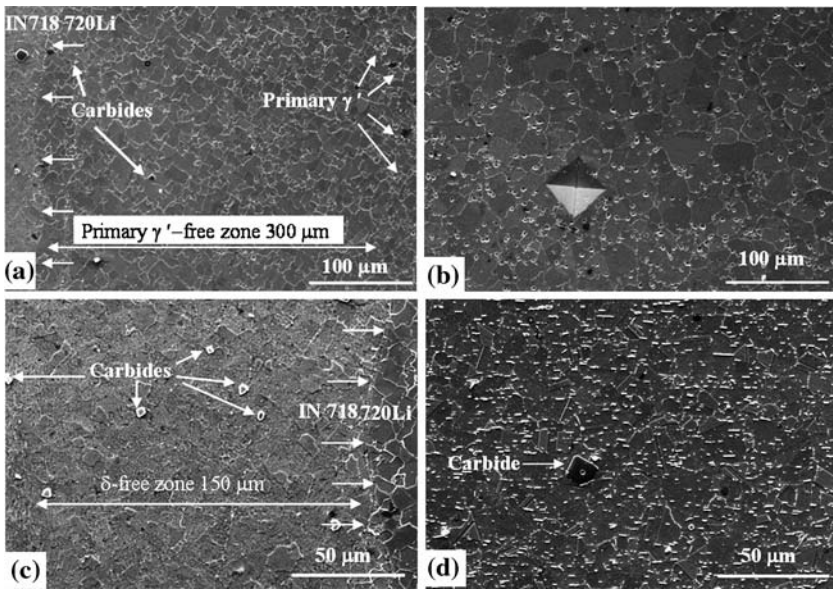

Fig. 1—SEM images showing (*a*) the as-welded U 720Li at the weld line and (*b*) the parent 720Li; (*c*) the as-welded IN 718 at the weld line; and (*d*) the parent IN 718. The weld line is arrowed, and the primary γ'-free zone in (a), the δ-free zone in (c), and carbides identified are indicated.

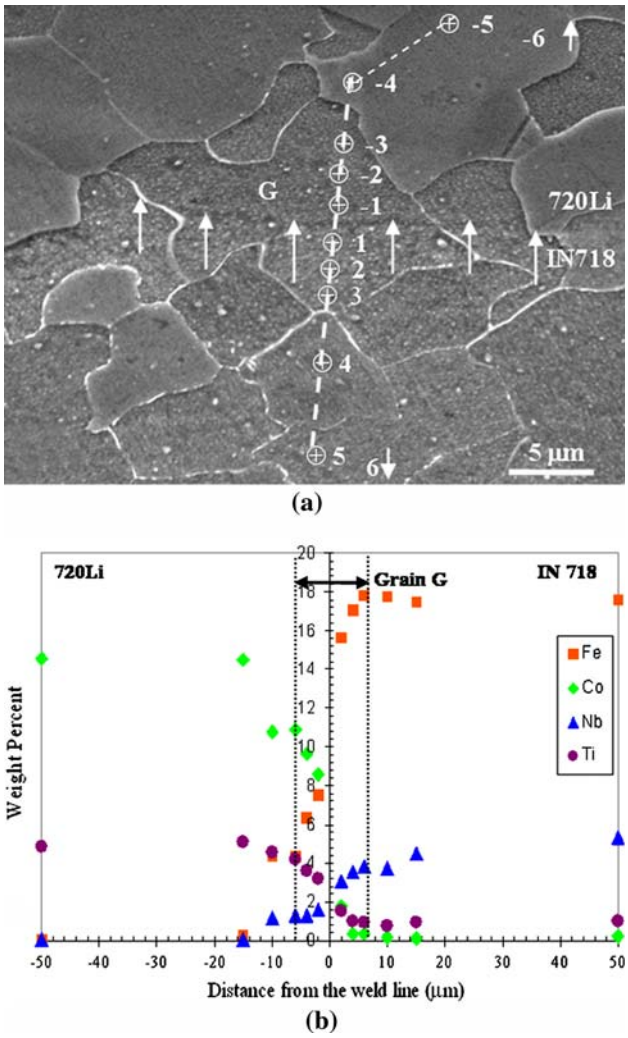

Fig. 2—(*a*) EDX spot analyses across the weld line (arrowed) on both sides at 2 to 50 mm from the weld line. The first three were conducted in the grain G, which is extended across the weld line. (*b*) The corresponding element profiles across the weld line. Refer to the text for the details.

in Figure 2(b). It is interesting to note that the EDX spot analysis across the boundary grain G seems to suggest a chemical gradient over 12 μm within this grain, where the chemical composition of the grain gradually changes from a typical alloy 720Li composition to an IN718 composition. This is most clearly seen for the alloying elements Fe and Co, because they are only present in IN718 and the latter only in alloy 720Li. Similar sharp chemical gradients across the weld line were found in different locations of the weld line. The analysis indicates that during IFW no significant cross weld diffusion processes take place, limiting the range of chemical variation from one to the other alloy to a range of one to two grains (less than 15 μm).

C. *Microhardness Profiles*

Figure 3 shows microhardness profiles across the weld line as a function of axial position for the as-welded and four 760 °C PWHT conditions. In the as-welded condition, alloy 720Li and IN718 base materials exhibit an average microhardness of 490 and 450 HV, respectively. In alloy 720Li, the microhardness profiles of the as-welded and PWHT'd conditions start changing around 7 mm from the weld line displaying a slight hardness increase in all cases but most noticeably in the as-welded condition. A significant difference between the as-welded and PWHT'd condition is seen in alloy 720Li with the hardness profile of the as-welded condition displaying a hardness trough at 2.5 mm from the weld line and a hardness at the weld line similar to the base material. In contrast, the PWHT'd conditions display a 10 pct hardness increase toward the weld line compared to the base material without any hardness trough in the HAZ.

Compared to alloy 720Li, IN718 shows a far more substantial hardness drop between the weld line and 2.5 mm from it in the as-welded condition, with no recovery of the hardness toward the weld line. The as-welded and PWHT'd hardness profiles of IN718 indicate a HAZ of about 5 mm, which is slightly smaller than the HAZ of alloy 720Li. The PWHT at 760 °C results in a dramatic recovery of the HAZ microhardness for IN718 even after a relatively short heat treatment of 2 hours. The four PWHT'd conditions of IN718 display, similar to alloy 720Li, hardness profile increases in the HAZ toward the weld line, reaching maximum hardness values of about 10 to 15 pct above the corresponding parent material. Figure 3 displays a number of additional interesting details, which are worth noting. First, all microhardness profiles seem to suggest a slight hardness decrease very close toward the weld line. The reason for this is related to recrystallization of γ matrix grains and will be discussed in Section III–F. As can be seen in Figure 3, the PWHT at 760 °C results in no significant hardness loss of the base material in alloy 720Li. However, IN718, whose recommended maximum aging temperature is 732 °C,[22,23,24] displays a significant loss of hardness in the base material during PWHT. The reason for the relatively high PWHT temperature is related to the difficulty of residual stress relieving inertia friction-welded alloy 720Li.[25] Microhardness profiles indicate that, from a mechanical property point of view, a PWHT at 760 °C should be kept as short as possible. However, residual stress analysis might suggest longer annealing times.

D. *Characterization of the γ' Distribution in Inertia-Welded Alloy 720Li*

Alloy 720Li is generally characterized by a trimodal distribution of γ' particle sizes, in which primary, secondary, and tertiary γ' particles are of different size ranges.[17] The three categories of γ' are termed parent γ' in this article, because all of them are originally present in parent alloy 720Li. Because each γ' family precipitates in a different temperature range, it is assumed that the chemical composition between the three γ' families is slightly different. Due to the chemical variation of γ', it is believed that tertiary γ' exhibits the lowest solvus temperature followed by secondary and primary

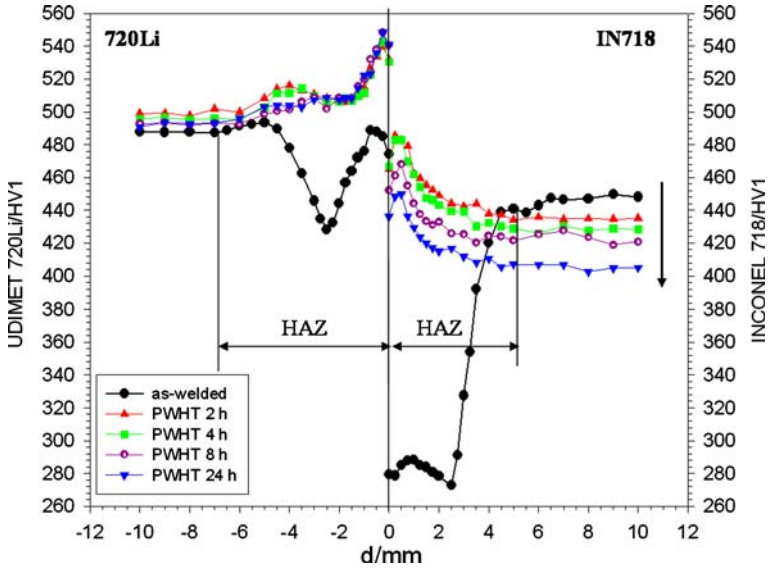

Fig. 3—Microhardness profiles of as-welded and 760 °C PWHT'd alloy 720Li and IN718 welds as a function of axial distance from the weld line ($d = 0$).

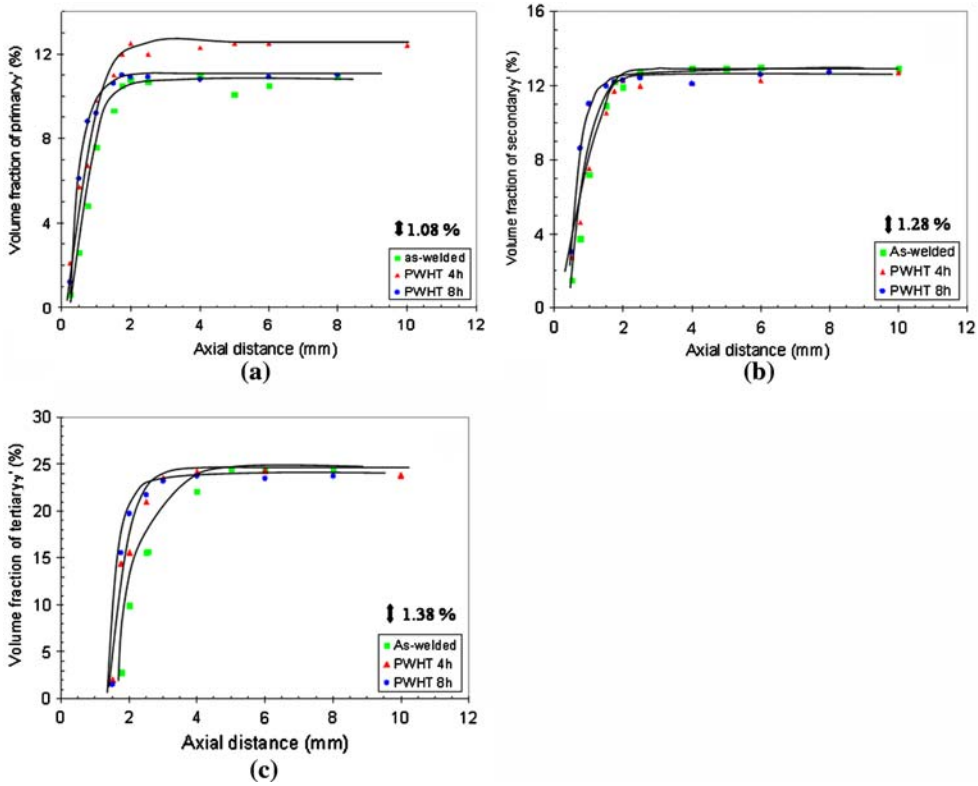

Fig. 4—Volume fraction profiles of (*a*) primary, (*b*) secondary, and (*c*) tertiary γ' against the axial position for the as-welded and PWHT (760 °C) conditions. A typical error bar is included in each plot, showing the average error of the volume fraction measurements.

γ'.[16,17,26] Under rapid heating and cooling conditions, it seems likely that due to the different size ranges of primary, secondary, and tertiary γ', such differences in solvus temperature will increase, which is attributed to a kinetic effect.

The distribution of intergranular and intragranular γ' typically observed in the parent material was studied as a function of position between the weld line and 10 mm from it for the as-welded and PWHT'd conditions using a FEGSEM. The particle size distribution typically varied between 1 to 4 μm for primary γ', 150 to 500 nm for secondary γ', and 30 to 70 nm for tertiary γ'. Figures 4(a) through (c) presents the volume fraction profiles of primary (a), secondary (b), and tertiary γ' (c) as a function of position from the weld line for the as-welded and two different PWHT'd conditions (4 and

Table III. Distribution of Parent γ' (Primary, Secondary, and Tertiary γ') in As-Welded and PWHT'd Alloy 720Li

Conditions	Parent γ'-Free Zone Size			Parent γ'-Depleted Zone Size		
	Primary γ' (mm)	Secondary γ' (mm)	Tertiary γ' (mm)	Primary γ' (mm)	Secondary γ' (mm)	Tertiary γ' (mm)
As-welded	0.25	0.5	1.75	1.75	2	5
4 h/760 °C PWHT	0.25	0.5	1.5	1.75	2	3.5
8 h/760 °C PWHT	0.25	0.5	1.5	1.75	2	2.5

8 hours at 760 °C). It can be seen from Figures 4(a) through (c) that the total volume fraction of γ' in the parent alloy 720Li studied is about 48 vol pct. Figures 4(a) through (c) clearly demonstrate that IFW has caused significant dissolution of all categories of γ' present in the parent material. Toward the weld line, first tertiary γ' dissolves, followed by secondary and last primary γ'. In the as-welded condition, the position where each γ' family has gone into solution is 0.25 mm from the weld line for primary γ', 0.5 mm from the weld line for secondary γ', and 1.75 mm from the weld line for tertiary γ'. The positions where each γ' family reach the volume fraction of the parent material are about 1.75 mm from the weld line for primary γ', about 2 mm from the weld line for secondary γ', and about 5 mm from the weld line for tertiary γ'. The positions of parent γ' families becoming absent or depleted in the HAZ are summarized in Table III.

It should be noted that in the HAZ of alloy 720Li, a fourth category of γ' was observed, previously termed reprecipitated γ',[13] which precipitated in high density upon cooling at the end of IFW and displays a mean particle size of less than 10 nm in the as-welded condition. Therefore, Table III summarizes the dissolving of parent γ' (*i.e.*, γ' originally present in the parent alloy 720Li) only.

As one would expect, the size of parent γ'-free zone and parent γ'-depleted zone for each family is strongly dependent on the precipitation size range. Also noted is that the degree to which PWHTs affect the γ' distribution along axial distance is strongly dependent on the precipitation size range as well. It is found that both PWHT schemes used have no influence on the primary and secondary γ' distribution. As mentioned in Section III–A, the solvus of primary γ' is around 1150 °C, well above the PWHT temperature (760 °C). Therefore, primary γ' is stable at the temperature of the PWHT (Figure 4(a)). The average accuracy of the primary γ' volume fraction was determined to be 1.08 vol pct. Note that the slightly higher volume fraction of primary γ' in the base material of the 4-hour PWHT condition compared to the other conditions is most likely due to inhomogeneity problems often observed in forged alloy 720Li.[27] Figure 4(b) indicates that a PWHT of 8 hours at 760 °C might have a slight effect on the secondary γ' volume fraction in the region of γ' depletion. The slightly larger volume fractions of secondary γ' suggest that some noticeable precipitation growth of secondary γ' is apparent in this region, although the difference could be well within the range of scatter. The average accuracy of secondary γ' volume fraction was determined to be 1. 28 vol pct. The quantitative microstructural analysis of alloy 720Li suggests that tertiary γ' starts to dissolve around 5 mm from the weld line (Figure 4(c) and Table III), although the microhardness already starts to change around 7 mm from the weld line. The average accuracy of tertiary γ' volume fraction was determined to be 1.38 vol pct, which indicates that small variations of the tertiary γ' volume fractions are unlikely to be detected. The volume fraction of tertiary γ' is reduced significantly as moving toward the weld line. As indicated in Figure 4(c), the volume fraction of tertiary γ' at 2.5 mm from the weld line has dropped from about 25 to 15 pct. Figure 4(c) also demonstrates that in the region of partly dissolved tertiary γ' (2 to 5 mm from the weld line), the PWHT has a significant influence on the volume fraction profile. Although the parent γ'-free zone size is not much reduced, the parent γ'-depleted zone size is reduced significantly (Table III), which appears to be caused by widespread growth of partially dissolved tertiary γ' particles.

When comparing Figure 3 with Figure 4(c), it becomes apparent that the loss of hardness between about 5 and 2 mm from the weld line for the as-welded alloy 720Li is strongly related to the depletion of tertiary γ', because primary and secondary γ' show no variation of the volume fraction in this region. Toward the weld line, the microhardness recovers, forming a characteristic "V"-type curve. The increase of strength in the region where most or all parent γ' was dissolved during joining is attributed mainly to the massive reprecipitation of ultrafine γ' precipitates. High-resolution FEGSEM work shows that, in the heat-affected zone, reprecipitation of γ' takes places during cooling at the end of the welding process. The reprecipitated γ' in alloy 720Li (less than 10 nm) is significantly smaller than tertiary γ' in the parent material (30 to 70 nm) due to the severe cooling rates and can therefore be easily distinguished from tertiary γ' during microstructural investigation. Figures 5(a) through (d) are typical high-magnification FEGSEM images under the as-welded condition, which show reprecipitated γ' particles at the weld line and 1.75 mm from the weld line and also show tertiary γ' particles at 1.75, 2.5, and 6 mm from the weld line, respectively. With the ability of high-resolution FEGSEM, the volume fraction of reprecipitated γ' in the as-welded condition was determined between the weld line and 5 mm from it. A volume fraction profile of reprecipitated γ' precipitates against the axial distance under the as-welded condition is produced and shown in Figure 6. The relatively high volume fraction of reprecipitated γ' at the weld line can be clearly seen in

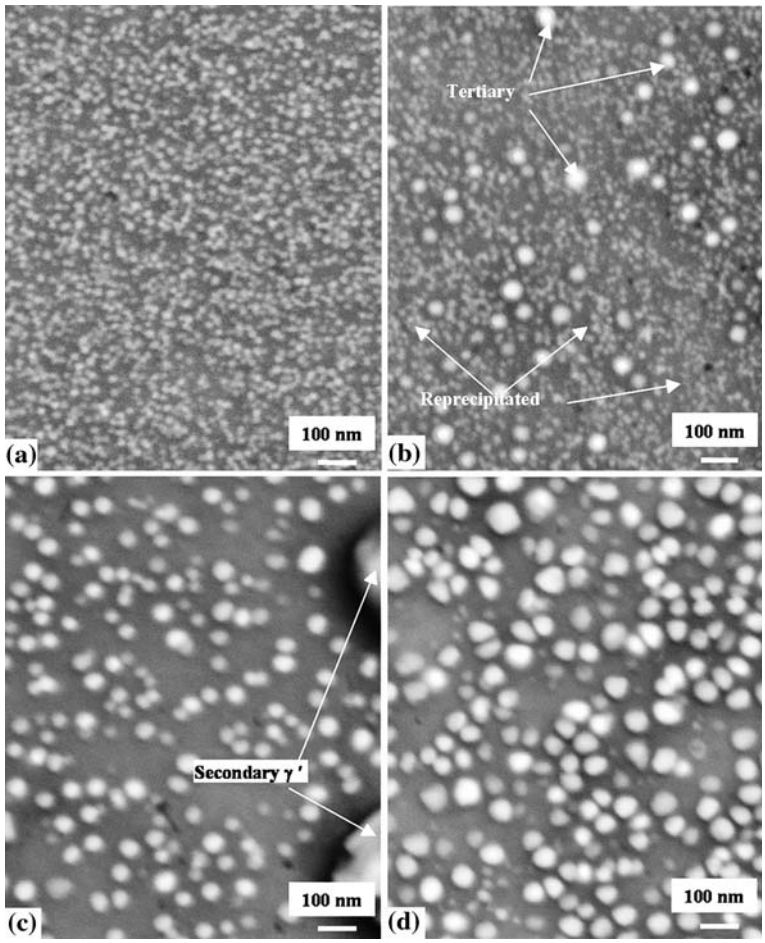

Fig. 5—The fine γ' precipitates (*a*) at the weld line, (*b*) 1.75 mm, (*c*) 2.5 mm, and (*d*) 6 mm from the weld line in as-welded alloy 720Li.

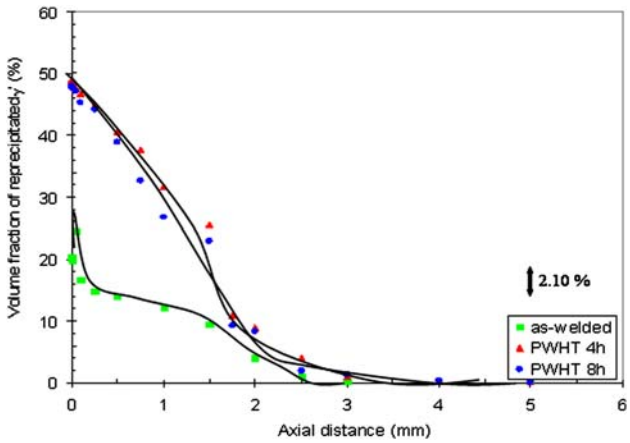

Fig. 6—Volume fraction profiles of reprecipitated γ' against the axial position for as-weld and PWHT (760 °C) conditions. A typical error bar is included, showing the average error of the volume fraction measurements.

Figure 5(a). The volume fraction of reprecipitated γ' at the weld line is measured to be 25 vol pct, and its average particle size is 9.4 nm by quantitative image analysis. The volume fraction of reprecipitated γ' reduces with increasing distance from the weld line, because some tertiary γ' particles are retained (Figure 5(b)). At 2.5 mm from the weld line, where a hardness trough in the as-welded condition is observed, the Figure 5(c) indicates no reprecipitated γ'. Clearly, it is difficult to judge if indeed no reprecipitation is apparent in this region, because the reprecipitated γ' might be too small to be resolved by FEGSEM studies. Additional TEM studies at 2.1 mm from the weld line (Figure 7) indicate ultrafine γ' in the range of a few nanometers. However, it seems reasonable to assume that such fine γ' only provides very limited strengthening, because it can be easily cut by dislocation.[17] As discussed earlier, at 2.5 mm from the weld line, the volume fraction of tertiary γ' has dropped from about 25 to 15 pct. Figure 5(c) reveals that the decrease in volume fraction at this position is mainly caused by partial dissolution of tertiary γ'. Compared with the tertiary γ' near the parent alloy (Figure 5(d)), the average particle size is reduced from 45 nm at 6 mm axial position to 30 nm at 2.5 mm. The importance of tertiary γ' in terms of strengthening has been previously reported for alloy 720Li in References 17 and 28. The present work supports these observations because the hardness trough observed in Figure 3 is clearly related to a reduced volume fraction and reduced particle size of tertiary γ'.

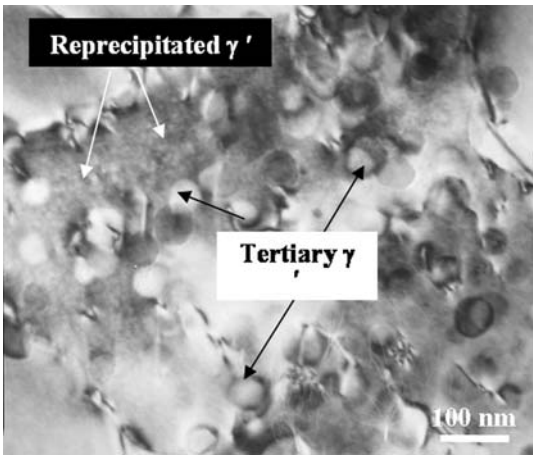

Fig. 7—A BF TEM micrograph showing both the reprecipitated and tertiary γ' at 2.1 mm from the weld line in as-welded U 720Li.

Previous high energy X-ray synchrotron diffraction[13] and the present quantitative analysis of γ' recorded by FEGSEM have demonstrated that the driving force for reprecipitation of ultra-fine γ' in the HAZ is provided by dissolution of parent γ' and is largest where all parent γ' has been dissolved during welding, *i.e.*, near the weld line. Therefore, the hardness trough observed in the as-welded condition can be attributed to a region of maximum γ' depletion. Such a region might be a few millimeters from the weld line (*e.g.*, 2.5 mm in this study), where the temperature during welding has partly dissolved parent γ', which does not provide sufficient reprecipitation driving force. However, the location of such a γ'-depleted zone can be expected to be dependent on the size of the HAZ. In fact, any particular microstructure features observed after welding will depend on temperature/stress history, which is determined by welding parameters.

During postweld heat treating the weld at 760 °C, the partially dissolved tertiary γ' coarsens, resulting in a tertiary γ' volume fraction close to 25 pct at 2.5 mm from the weld line. As a result, no hardness trough is observed in this region (Figure 3). Assuming that a 760 °C PWHT of inertia friction-welded alloy 720Li results in a fully reprecipitated γ' microstructure after 4 hours (confirmed for 8 hours at 760 °C[13]), it was possible to calculate the volume fraction of the reprecipitated γ' precipitates. The total volume fraction of γ' in the parent material (parent γ') had been calculated to be 48 pct. The volume fraction of reprecipitated γ' at a specific axial position is the total volume fraction (*i.e.*, 48 pct in this study) minus the volume fraction of parent γ' (primary, secondary, and tertiary γ') at that position. As one leaves the weld line, the volume fractions of retained parent γ' increase while the volume fraction of reprecipitated γ' decreases. The volume fraction of reprecipitated γ' drops to zero around 5 mm from the weld line, where 48 vol pct of parent γ' has been recorded. The obtained distribution profiles of the reprecipitated γ' for both PWHT'd conditions alongside the as-welded condition are plotted in Figure 6. It can be seen in Figure 6 that the two PWHT curves display a steep gradient from ~2.5 mm toward the weld line, demonstrating that the volume fraction of reprecipitated γ' increases dramatically within this region during PWHT, which coincides with the dramatic increase in microhardness shown in Figure 3. The dramatic hardness increase in this region should be also attributed to slightly coarsening of reprecipitated γ'.

E. *Characterization of the γ'' Distribution in Inertia-Welded IN718*

Because it was not possible to visualize γ'' in a FEGSEM, the microstructural characterization of the main strengthening phase γ'' in IN718 was undertaken using TEM. The strengthening phase γ'' in IN718 generally precipitates in a disc shape with the disc plane being parallel to the $\{100\}_\gamma$matrix planes.[29–32] In order to reveal the true γ'' disc diameter, all TEM micrographs were taken along the $\{100\}_\gamma$ zone axis. In view of partial strengthening contribution from γ', the distribution of γ' in IN718 was also characterized using FEGSEM.

Figures 8(a) through (d) are bright-field (BF) TEM images together with the corresponding selected area diffraction patterns (SADPs) along the $(001)_\gamma$ zone axis, showing the as-welded microstructure at 0.2 mm (a), 0.7 mm (b), 2.1 mm (c), and 4 mm (d) from the weld line. Between 0.2 and 2.1 mm from the weld line, the BF images reveal no γ' and γ'' precipitates. In addition, the SADPs at these locations show no superlattice reflections, indicating that indeed both γ' and γ'' have been fully dissolved. At 4 mm from the weld line, the BF image shows a fine γ'' distribution. The real size of the γ'' is not possible to be measured under BF condition, but work in CDF images suggests the γ'' precipitates in parent IN718 are about 5 nm in thickness and 10 to 20 nm in length. It is believed that the mottled contrast seen in Figure 8(d) is a result of misfit strain between γ'' and the γ matrix. The dissolution of the γ'' strengthening phase between the weld line and about 2 mm from it explains the dramatic loss of strength in this region (Figure 3). The BF TEM images also show a high population of weakly paired dislocations (arrowed in Figure 8(b)) near the weld line.

The totally dissolved γ'' in the near-weld region is reprecipitated fully as thin ellipsoidal disc-shaped particles after PWHT for 8 hours at 760 °C. Figures 9(a) and (b), using CDF images and SADPs, display the γ'' distribution in IN718 at 0.2 and 8 mm from the weld line after postweld heat treating the weld for 8 hours at 760 °C. Both images show a much coarsened but relatively similar γ'' size (70 nm on average for both locations), even though they have been exposed to very different temperatures and cooling rates during the IFW process. This result is somewhat surprising, especially because the strong influence of the temperature history on the γ' distribution can be observed on the inertia friction-welded alloy 720Li side. However, one should keep in mind that the γ'' particles are generally very fine similar to tertiary γ'. The chosen PWHT temperature of 760 °C causes substantial γ'' coarsening, which can be seen when comparing Figures 8(d) and 9(b) and in the form of loss of strength in Figure 3. It therefore seems

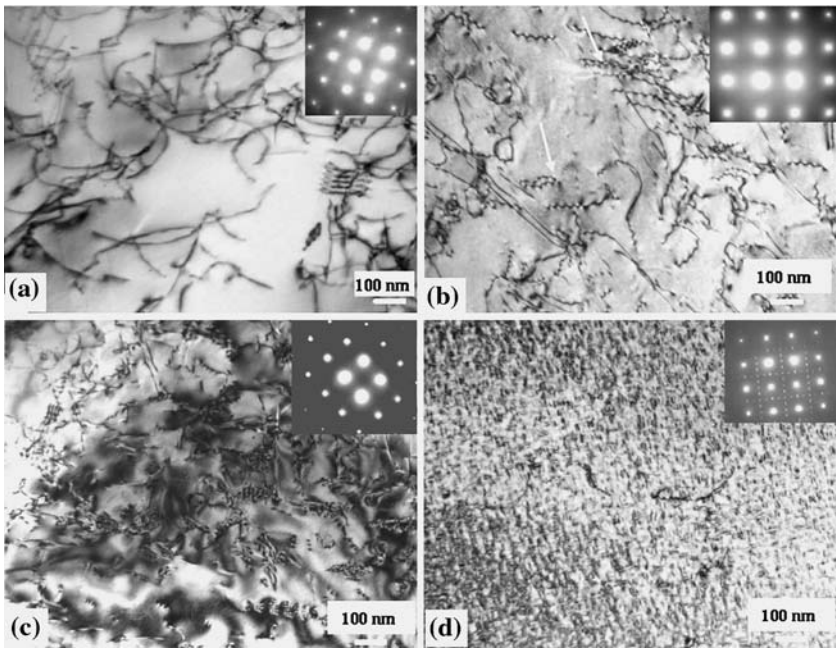

Fig. 8—TEM micrographs showing the microstructure and diffraction pattern of as-welded IN 718: (*a*) 0.2 mm, (*b*) 0.7 mm, (*c*) 2.1 mm, and (*d*) 4 mm away from the weld line.

that during substantial overaging of γ'' at high annealing temperatures, the γ'' in the weld line region catches up with the γ'' of the parent material in terms of particle size distribution. The PWHT scheme is applied to relieve the residual stress induced by the IFW process, but it can be an overaging scheme to the IN718 in terms of its strengthening/hardening effect, as evidenced by the microhardness decrease from 450 to 420 HV1 for the base alloy IN718.

The CDF images shown in Figures 9(a) and (b) were obtained from TEM regions of a similar thickness after heat treating the material for 8 hours at 760 °C. The CDF image in (a) was taken with the $[001]_\gamma$ beam axis using $\mathbf{g} = [1/2 10]_{\gamma''}$, showing the $[100]_{\gamma''}$ variant only; while the image in Figure 9(b) was taken using $\mathbf{g} = [1\frac{1}{2} 0]_{\gamma''}$, showing the $[010]_{\gamma''}$ variant only. It was found that the γ'' in the near weld region showed a density noticeably higher than that in the base alloy after PWHT. A series of quantitative image analysis was conducted on these CDF images from the near weld line region to the base alloy region for γ'' volume fraction. A volume fraction profile of γ'' against axial distance from the weld line is given in Figure 10, which shows that the γ'' volume fraction at the weld line is 7 pct higher than that in the base alloy. In the weld line region (0.2 mm from the weld line), the volume fraction of γ'' particles is 22.6 vol pct after 8 hours at 760 °C, which reduces to 19.5 vol pct at 1.3 mm and 16.2 vol pct at 2.5 mm from the weld line. In the parent material of IN718, γ'' was determined to have a volume fraction of about 15.5 vol pct. The reason for such a considerably higher volume fraction of γ'' particles near the weld line compared to the parent material can be attributed to the dissolution of δ phase in the weld line region, as observed and shown in Figure 1(b). The dissolution of δ phase provides additional Nb for reprecipitation of γ'' during PWHT, which explains the hardness increase toward the weld line in the PWHT'd condition of IN718 (about 10 pct above the parent material after 8 h/760 °C, Figure 3).

A small amount of fine γ' precipitates was observed in the IN718 after the 8 h/760 °C PWHT. Figure 11 exhibits the morphology and distribution of the γ' precipitates at the weld line and 5 mm from it in IN718 after 8 hours at 760 °C. The γ' precipitation size is about 10 to 20 nm in diameter. At the weld line, the γ' precipitates display a slightly higher volume fraction (6.4 pct) than in the parent material (4.4 pct). Following an image analysis of a series of image from different locations, it was possible to determine the volume fraction of γ' against the axial distance from the weld line for IN718 after 8 hours at 760 °C (Figure 10). It can be seen that both γ' and γ'' show higher volume fraction in the weld line region than in the parent material and that the location of the increase for both phases coincides reasonably well with the location of the hardness increase seen in Figure 3. The reason for the increased volume fraction of γ' precipitates in the near weld line region is not entirely obvious, but it might be related to the dissolution of Ti-rich carbides in this region.

F. *Characterization of the Grain Size Distribution and Plastic Work across the Weld Line*

The change in grain size across the weld line is summarized in Figure 12 for the as-welded condition. It was found that on both sides of the bond the grain size starts to change around 2 mm from the weld line. In each alloy, a grain size trough is observed around 0.5 mm from the weld line with alloy 720Li displaying a

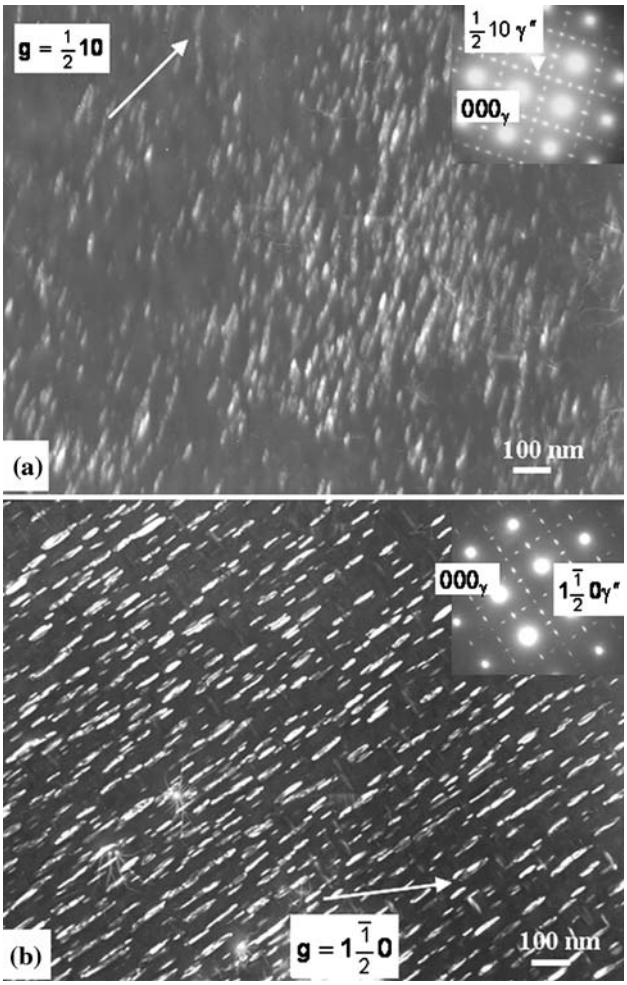

Fig. 9—Centered dark-field TEM micrographs and diffraction patterns showing the γ'' precipitates in IN718 after 8 h/760 °C PWHT: (*a*) 0.2 mm and (*b*) 8 mm away from the weld line.

grain size of about 8 μm compared to 15 μm in the parent material and IN718 having a grain size of 7 μm compared to 10 μm in the parent material. The parent material of both alloys displays a substantial number of

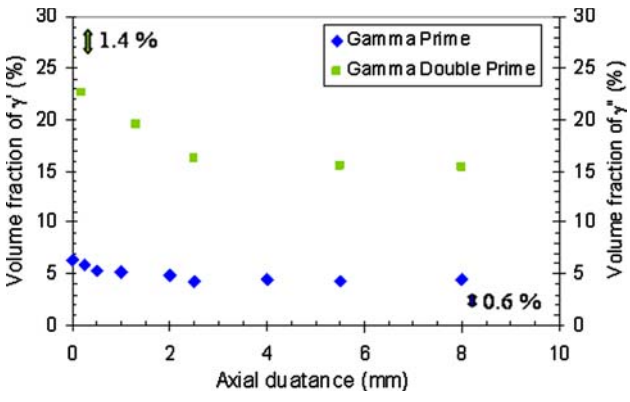

Fig. 10—The volume fraction of γ' and γ'' particles against the axial distance in the IN 718 subjected to 8 h/760 °C PWHT. Error bars are included, showing the average error of the volume fraction measurements.

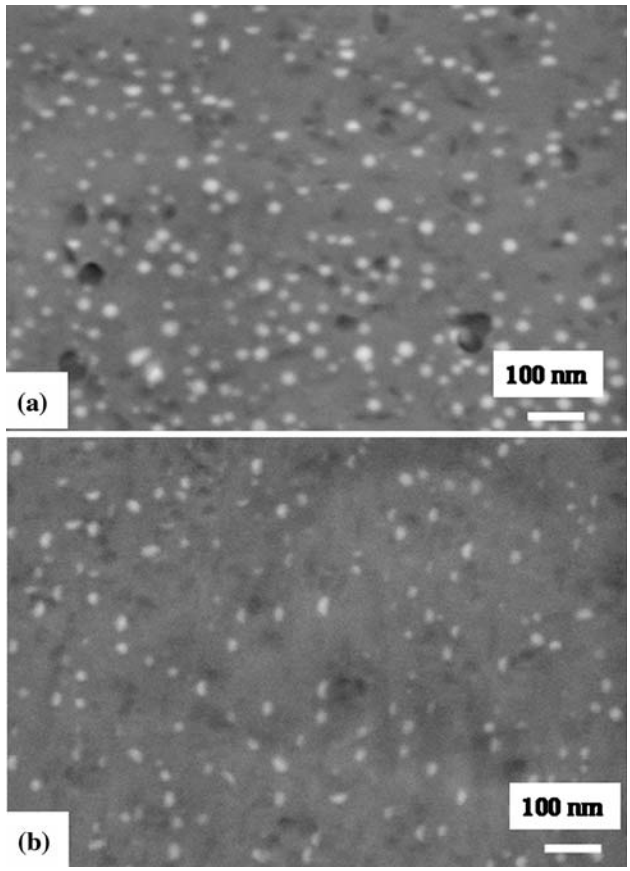

Fig. 11—FEGSEM micrographs showing the fine γ' particles in the 8 h/760 °C PWHT'd IN 718: (*a*) at the weld line and (*b*) 5 mm away from the weld line.

twins. In order to assess the level of plastic work stored in the material at various axial positions, the change in stored energy across the weld line is also shown in Figure 12. The profile indicates that the region of the grain size troughs coincides with high stored energy levels. At the weld line, the stored energy drops to a similar value, as observed in the parent material. This

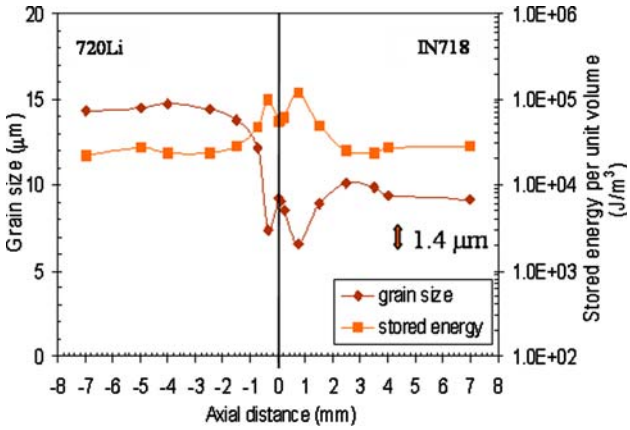

Fig. 12—The grain size distribution and the change in stored energy across the weld line in the as-welded alloy 720Li to IN718. An error bar is given for the grain size measurements.

result suggests that in the weld line region, the material was sufficiently hot and plastically deformed during IFW to recrystallize during cooling. The regions at 0.5 mm from the weld line represent the area where recrystallization has just started, resulting in a refined grain size. This observation is in good agreement with what has been previously reported for inertia friction-welded RR1000.[12] The fully recrystallized microstructure in conjunction with a slightly coarsened grain size compared to 0.5 mm from the weld line explains the slight hardness drop in this region seen for all conditions in Figure 3. Although grain size and stored energy analysis have not been carried out for the PWHT'd conditions, it is fair to assume that an annealing temperature of 760 °C will not result in any additional recrystallization on either side of the heat-affected zone.

IV. SUMMARY

In this article, the microstructures of as-welded and variously PWHT'd alloy 720Li to IN718 inertia friction welds have been studied in detail. Hardness profiles have been recorded in order to map the variation of strength across the weld line of the dissimilar joint. Subsequently, the microstructure has been studied by means of SEM and TEM as well as EBSD. The main findings can be summarized as follows.

1. The microhardness profiles suggest that the heat-affected zone in alloy 720Li is slightly larger than in IN718. This is believed to be due to different high-temperature mechanical properties of the two alloys. IN718 will be ejected from the weld region into the flash at a lower temperature than alloy 720Li. As a result, the material in the weld line region of alloy 720Li is exposed to a higher temperature and longer time than IN718.
2. In the as-welded condition, the two nickel-base superalloys display substantial microhardness differences in the HAZ. The high γ' volume fraction alloy 720Li exhibits a strength trough near the weld line, with the microhardness being 80 pct of the parent material, while IN718 displays a soft region between the weld line and ~2 mm from it where the microhardness is only 50 pct of the parent material. The differences in hardness profiles can be understood in terms of γ' dissolution and reprecipitation during IFW. Due to the high levels of Al and Ti in alloy 720Li, this kind of alloy has a large driving force to reprecipitate γ' at the end of IFW during quenching. As a result, alloy 720Li shows no precipitation-free zone in the as-welded condition. On the other hand, IN718 has a comparatively low volume fraction of γ' due to low levels of Al and Ti. No significant γ' reprecipitation takes place at the end of IFW, although all γ' and γ'' have gone into solution, resulting in the aforementioned soft zone.
3. In alloy 720Li, the hardness profiles in the as-welded and PWHT'd conditions are mainly influenced by the tertiary and reprecipitated γ' distribution. At around 5 mm from the weld line, the volume fraction of the parent γ' starts to decrease due to tertiary γ' being dissolved. Closer to the weld line, also secondary and primary γ' are being dissolved, gradually increasing the driving force for γ' reprecipitation toward the weld line. The hardness trough in the microhardness profile of the as-welded alloy 720Li is a γ'-depleted zone, where the strengthening tertiary γ' phase has been largely dissolved but no sufficiently large volume fraction of reprecipitated γ' is present. Between 2 mm from the weld line and the weld line, the volume fraction of reprecipitated γ' raises dramatically due to the dissolution of primary and secondary γ'. This results in the microhardness increasing toward the weld line. The PWHT results in coarsening of reprecipitated and tertiary γ' and the disappearance of the γ' depleted zone.
4. In IN718, the hardness profile in the HAZ is characterized by a pronounced hardness drop between the weld line and ~2 mm from it to 50 pct, compared to the parent material. The TEM studies have demonstrated that, in this soft region, all of the strengthening γ'' has gone into solution and not reprecipitated during cooling. When γ'/γ'' is dissolved at high temperature, the low levels of Ti and Al do not create a large enough driving force for reprecipitation during quenching at the end of the IFW process. The PWHT at 760 °C results in the formation of an increased γ'' volume fraction in the previously soft zone compared to the parent material due to dissolution of δ particles (a small increase in γ' population is also observed here), producing a hardness increase toward the weld line. The substantial coarsening of γ'' in the HAZ and the parent material after PWHTs reduces the overall hardness of the material. The degree of coarsening and loss of strength is, as one would expect, dependent on the holding time during the PWHT. After 8-hour PWHT, the coarsening of γ'' has resulted in a similar γ'' particle size in the near weld line region and the parent material.
5. The EBSD studies of the grain size distribution and the stored energy across the weld line show that, in the near weld line region, alloy 720Li and IN718 - have recrystallized during the welding process. Both sides of the weld line display a region about 0.5 mm from the weld line with a significantly refined grain size due to the onset of recrystallization. At the weld line, the grain size has increased again due to grain growth after recrystallization. This, together with the reduced stored work observed at the weld line, explains the slight hardness drop observed in all microhardness profiles at the weld line.

ACKNOWLEDGMENTS

The authors acknowledge the UK Department of Trade and Industry and Rolls Royce plc. for financial support and Peter Thornton (The University of

Birmingham) and Mike Faulkner (University of Manchester) for experimental support.

REFERENCES

1. R. Vincent: *Acta Metall.*, 1985, vol. 33, pp. 1205–16.
2. A. Lingenfelter: in *Superalloy 718—Metallurgy and Applications*, E.A. Loria, ed., TMS, Warrendale, PA, 1989, pp. 673–83.
3. S. Gobbi, Li Zhang, J. Norris, K.H. Richter, and J.H. Loreau: *J. Mater. Proc. Technol.*, 1996, vol. 56, pp. 333–45.
4. R.G. Thompson, B. Radhakrishnan, and D.E. Mayo: in *Superalloy 718—Metallurgy and Applications*, E.A. Loria, ed., TMS, Warrendale, PA, 1989, pp. 437–55.
5. B. Radhakrishnan and R.G. Thompson: *Metall. Trans. A*, 1993, vol. 24A, pp. 1409–22.
6. M. Qian and J.C. Lippold: *Acta Mater.*, 2003, vol. 51, pp. 3351–61.
7. O.A. Ojo, N.L. Richards, and M.C. Chaturvedi: *Scripta Mater.*, 2004, vol. 51, pp. 683–88.
8. N.C. Sekhar and R.C. Reed: *Sci. Technol. Weld. Join.*, 2002, vol. 7, pp. 77–87.
9. K.K. Wang: *Weld. Res. Counc. Bull.*, 1975, vol. 204, pp. 1–22.
10. R. Spinat and Y. Honnorat: in *High Temperature Alloys for Gas Turbines and Other Applications*, W. Betz, R. Brunetaud, D. Coutsouradis, H. Fischmeister, T.B. Gibbons, I. Kvernes, Y. Lindblom, J.B. Marriott, and D.B. Meadowcroft, eds., Dordrecht D. Reidel, Butterworth-Heinemann, Ltd., Oxford, 1986, pp. 151–57.
11. J.C. Williams and E.A. Starke, Jr.: *Acta Mater.*, 2003, vol. 51, pp. 5775–99.
12. M. Preuss, J.W.L Pang, P.J. Withers, and G.J. Baxter: *Metall. Mater. Trans. A*, 2002, vol. 33A, pp. 3215–25.
13. M. Preuss, J. Quinta da Fonseca, I. Kyriakoglou, P.J. Withers, and G.J. Baxter: in *Superalloys 2004*, K.A. Green, T.M. Pollock, H. Harada, T.F. Howson, R.C. Reed, J.J. Schirra, and S. Walston, eds., TMS Warrendale, PA, 2004, pp. 477–84.
14. M. Preuss, J.W.L. Pang, P.J. Withers, and G.J. Baxter: *Metall. Mater. Trans. A*, 2002, vol. 33A, pp. 3227–34.
15. J.W.L. Pang, M. Preuss, P.J. Withers, G.J. Baxter, and C. Small: *Mater. Sci. Eng. A*, 2003, vol. A356, pp. 405–13.
16. M. Soucail and Y. Bienvenu: *Mater. Sci. Eng. A*, 1996, vol. A220, pp. 215–22.
17. M.P. Jackson and R.C. Reed: *Mater. Sci. Eng. A*, 1999, vol. A259, pp. 85–97.
18. Software and user manual at http://www.umist.ac.uk/material/reserach/aluminum/ frame.html.
19. D.U. Furrer and H.-J. Fecht: *Scripta Mater.*, 1999, vol. 40, pp. 1215–20.
20. L. Wang, M. Preuss, P.J Withers, G. Baxter, and P. Wilson: *Metall. Mater. Trans. B*, 2005, vol. 36B, pp. 513–23.
21. J.W. Brooks: *Mater. Des.*, 2000, vol. 21, pp. 297–303.
22. D.R. Muzyka and G.N. Maniar: *Metals Engineering Quarterly*, ASM, Cleveland, OH, 1969, pp. 23–37.
23. D.J. Wilson: *Trans. ASME*, 1973, Apr., pp. 112–23.
24. H.F. Merrick: *Metall. Trans. A*, 1976, vol. 7A, pp. 505–14.
25. M. Karadge, G. Regino, A. Hoerling, A. Korsunsky, P.J. Withers, D. Nowell, and M. Preuss: Manchester Materials Science Centre, University of Manchester, Manchester, United Kingdom, unpublished research, 2006.
26. R.A. Ricks, A.J. Porter, and R.C. Ecob: *Acta Metall.*, 1983, vol. 31, pp. 43–53.
27. R. Couturier, H. Burlet, S. Terzi, S. Dubitiez, L. Guetaz, and G. Raisson: in *Superalloys 2004*, K.A. Green, T.M. Pollock, H. Harada, T.F. Howson, R.C. Reed, J.J. Schirra, and S. Walston, eds., TMS, Warrendale, PA, 2004, pp. 351–59.
28. F. Torster, G. Baumeister, J. Albrecht, G. Luetjering, D. Helm, and M.A. Daeubler: *Mater. Sci. Eng. A*, 1997, vol. A234, pp. 189–92.
29. D.F. Paulonis, J.M. Oblak, and D.S. Duvall: *Trans. ASM*, 1969, vol. 62, pp. 611–22.
30. R. Cozar and A. Pineau: *Metall. Trans.*, 1973, vol. 4, pp. 47–59.
31. J.M. Oblak, D.F. Paulonis, and D.S. Duvall: *Metall. Trans.*, 1974, vol. 5, pp. 143–53.
32. J.F. Collier, S.H. Wong, J.C. Phillips, and J.K. Tien: *Metall. Trans. A*, 1988, vol. 19A, pp. 1657–66.